Tuning of Catalytic Activity by Thermoelectric Materials for Carbon Dioxide Hydrogenation

Abdenour Achour, Kan Chen, Michael J. Reece, and Zhaorong Huang*

An innovative use of a thermoelectric material (BiCuSeO) as a support and promoter of catalysis for CO_2 hydrogenation is reported here. It is proposed that the capability of thermoelectric materials to shift the Fermi level and work function of a catalyst lead to an exponential increase of catalytic activity for catalyst particles deposited on its surface. Experimental results show that the CO_2 conversion and CO selectivity are increased significantly by a thermoelectric Seebeck voltage. This suggests that the thermoelectric effect can not only increase the reaction rate but also change chemical equilibrium, which leads to the change of thermodynamic equilibrium for the conversion of CO_2 in its hydrogenation reactions. It is also shown that this thermoelectric promotion of catalysis enables BiCuSeO oxide itself to have a high catalytic activity for CO_2 hydrogenation. The generic nature of the mechanism suggests the possibility that many catalytic chemical reactions can be tuned in situ to achieve much higher reaction rates, or at lower temperatures, or have better desired selectivity through changing the backside temperature of the thermoelectric support.

1. Introduction

Thermoelectric (TE) materials have recently attracted widespread interest in research because they can convert a temperature difference directly into an electrical voltage via the Seebeck effect, $S = -V/\Delta T$, where V is the voltage between the two ends of the TE material and ΔT the temperature difference, S is the Seebeck coefficient. The performance of a TE material is ranked by its figure of merit $ZT = S^2\sigma T/\kappa$, where σ is the electrical conductivity, κ the thermal conductivity, and

T absolute temperature.[1] Most currently used TE materials are heavy-metal-based, such as Bi_2Te_3 and PbTe, due to their high ZT. However, these materials are not best suited for medium to high temperature, large scale applications, because of problems such as their low melting, or decomposition, or oxidation temperatures. They are also harmful to environment and contain scarce constituent elements. On the other hand, oxide TE materials, such as p-type layered BiCuSeO, cobalt oxide A_xCoO_2 (A = Na, Ca, Sr), and n-type $NaTaO_3$-Fe_2O_3, $CaMnO_3$ and $SrTiO_3$ based perovskites, can overcome these disadvantages.[2] TE devices are usually configured in modules by connecting the p-type and n-type TE legs electrically in series and thermally in parallel. We report here an innovative use of TE materials as a catalyst support and show its substantial promotional effect on catalytic activity. BiCuSeO (BCSO) was selected as the thermoelectric materials for this investigation because it possesses good TE properties to over 900 K, an extraordinary low intrinsic thermal conductivity of less than 0.5 W m^{-1} K^{-1}; therefore, a high temperature difference can easily built up across this material; high Seebeck coefficient up to 500 µV K^{-1} at room temperature and greater than 300 µV K^{-1} at high temperatures, and no decomposition below 773 K.[2]

Catalyst promoters improve the activity, selectivity, or lifetime of a catalyst and can generally be divided into structural and electronic promoters. Structural promoters enhance and stabilize the dispersion of the catalyst on the support. Electronic promoters induce changes of electronic state of the catalyst near the Fermi level.[3] These promoters are added and fixed during the catalyst preparation and therefore can be subject to degradation during the catalytic process. On the other hand, electrochemical promotion, also called non-Faradaic electrochemical modification of catalytic activity (NEMCA), which allows for controlled in situ introduction of promoters on catalyst surfaces under operating conditions.[3,4] NEMCA has proved to be an excellent research technique but its large scale industrial use has been limited due to its shortcomings: (i) low efficiency of catalyst materials (which are often expensive noble metals) because it requires a continuous electrode to maintain conductivity, (ii) need to maintain electrical connection under often harsh conditions, and (iii) the incompatibility of its reactor configuration (often a fuel cell configuration) with typical chemical reactors (fixed bed, monolithic, and fluidized bed).[5] We report here the realization of in situ, reversible, and significant modification of catalytic activity for both continuous

A. Achour, Dr. Z. Huang
Surface Engineering and Nanotechnology Institute
Cranfield University
Bedfordshire MK43 0AL, UK
E-mail: z.huang@cranfield.ac.uk
Dr. K. Chen, Prof. M. J. Reece
School of Engineering and Materials Science
Queen Mary
University of London
Mile End Rd, London E1 4NS, UK

🆔 The ORCID identification number(s) for the author(s) of this article can be found under https://doi.org/10.1002/aenm.201701430.

ADVANCED
SCIENCE NEWS
www.advancedsciencenews.com

ADVANCED
ENERGY
MATERIALS
www.advenergymat.de

thin film and highly dispersed (nanoscale particles) metal catalysts, by using TE materials as a catalyst support for CO_2 hydrogenation. Furthermore, we show that this profound promotional effect on catalytic activity by the TE effect also enables the oxide TE material itself to possess high catalytic activity for CO_2 hydrogenation.

The concentration of carbon dioxide in the atmosphere has risen from ≈280 ppm before the industrial revolution to ≈400 ppm in 2013 and is projected to be ≈500 ppm by 2050.[6] This contributes to the increase in global temperature and climate changes due to the "greenhouse effect." Hence there are extensive efforts to reduce CO_2 emissions around the world. Generally speaking, there are three strategies to achieve this: (i) reduce CO_2 production, (ii) storage, and (iii) usage. The first two options, which involve improving energy efficiency, switching to renewable energy, and CO_2 capture and sequestration, have been the major focus in the past. The third strategy, i.e., using CO_2 as a feedstock for making useful chemicals, is regarded as the most feasible and effective solution to our carbon conundrum.[7] The CO_2 hydrogenation may undergo two main processes, the first is the reverse water-gas shift (RWGS) reaction (Equation (1)) and the other leads to the formation of hydrocarbons (Equation (2))

$$CO_2 + H_2 \rightarrow CO + H_2O \tag{1}$$

$$xCO_2 + (2x - z + \gamma/2)H_2 \rightarrow C_xH_yO_z + (2x - z)H_2O \tag{2}$$

For $x = 1$, $\gamma = 4$, and $z = 0$ (i.e., the inlet gas ratio $CO_2/H_2 = 1:4$) one has the methanation reaction. RWGS reaction is one of the most established reactions to convert CO_2 into CO and H_2O, from which liquid hydrocarbons conversion via Fischer–Tropsch synthesis can be achieved.

2. Theoretical Consideration

NEMCA, which involves a reversible change of catalytic properties of metal catalysts deposited on solid electrolytes, can be obtained by applying a small external electric current or voltage. NEMCA is due to the back spillover of ionic species from electrolytes to form a double layer at the catalyst surface, which leads to a change of the work function and chemisorption properties of the catalyst.[3,8] The effective change of surface work function leads to an exponential change of chemical reaction,[9] i.e.,

$$Ln(r/r_o) = \alpha \Delta\phi / k_b T \tag{3}$$

where r is the new reaction rate, r_o is the open-circuit reaction rate, k_b is the Boltzmann constant, α is an empirically determined constants, and $\Delta\phi$ is the change of work function due to the applied external voltage. Under certain conditions, $\Delta\phi$ is linearly proportional to the non-Ohm drop of external potential.[3,4,9]

The basic idea of this work is to use a thermoelectric material to change the effective work function of catalyst particles to achieve a significant increase of the catalytic activity. First, consider the change of the Fermi level for TE material BCSO when there is a temperature change (**Figure 1**). BCSO is a p-type TE
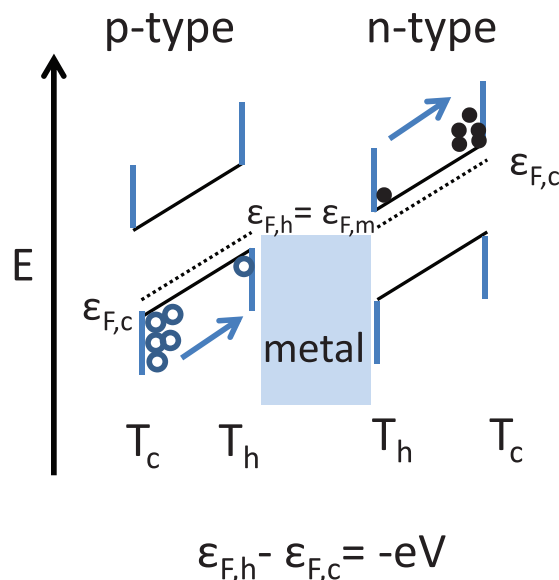
Figure 1. Energy levels of electrons in a thermoelectric material with a temperature gradient. Schematic diagram of energy bands and Fermi levels for p-type and n-type TE materials and a metal particle supporting on the TE materials at the hot side. T_c and T_h are the temperatures at the cold and hot ends, respectively. The arrow heads show the electric field direction within the TE material.

material, holes at the hot side diffuse into the cold side upon heating, forming an internal electrical field. Once equilibrium is reached the Fermi level (also called electrochemical potential) at the hot side $\varepsilon_{F,h}$ is higher than at the beginning and cold side $\varepsilon_{F,c}$ and $\Delta\varepsilon_F = \varepsilon_{F,h} - \varepsilon_{F,c} = -eV$, here $-e$ is the charge of an electron and V is the Seebeck voltage.

As no external charges exist, the change of the work function at the surface is the inverse change of the Fermi level, i.e., $\Delta\phi = -\Delta\varepsilon_F$, so $\Delta\phi = eV$ at the hot surface T_h. If a metal particle is deposited on the TE material, at the hot surface, its Fermi level $\varepsilon_{F,m}$ must be the same as the Fermi level of the TE at the surface, i.e., $\varepsilon_{F,m} = \varepsilon_{F,h}$ (Figure 1). Therefore, $\Delta\varepsilon_{F,m} = \Delta\varepsilon_F$ and the change of work function $\Delta\phi_m = eV$ is also true for metal particles supported on the TE material.

Apply the generalized dependence of catalytic rate on catalyst work function Equation (3), then we have

$$Ln(r/r_0) = -\gamma eV / k_b T \tag{4}$$

Here γ is a constant, to be determined by experiment. The introduction of a minus sign makes $-eV$ the extra energy of an electron at the surface due to the Seebeck voltage V. Combining Equation (4) and the definition of Seebeck coefficient S gives

$$Ln(r/r_0) = \gamma \cdot e \cdot S \cdot \Delta T / k_b T$$
$$= \gamma \cdot e \cdot S \cdot (T_h - T_c) / k_b T_h, \text{ at hot side } T_h \tag{5}$$

$$\text{And} \quad Ln(r/r_0) = \gamma \cdot e \cdot S \cdot \Delta T / k_b T$$
$$= \gamma \cdot e \cdot S \cdot (T_c - T_h) / k_b T_c, \text{ at cold side } T_c \tag{6}$$

when S is not a constant, $S(T_h - T_c)$ should be replaced by $\int_{T_c}^{T_h} S(T) dT$.

**ADVANCED
SCIENCE NEWS**

www.advancedsciencenews.com

**ADVANCED
ENERGY
MATERIALS**

www.advenergymat.de

Equations (4)–(6) link catalytic activity with Seebeck voltage and temperature for a metallic catalyst supported on a TE material.

3. Results and Discussion

3.1. Thermoelectric Property of BiCuSeO

Figure 2 shows the temperature dependence of (a) Seebeck coefficient and electrical conductivity, (b) thermal conductivity, and (c) power factor and dimensionless figure of merit ZT for

(a)

(b)

(c)
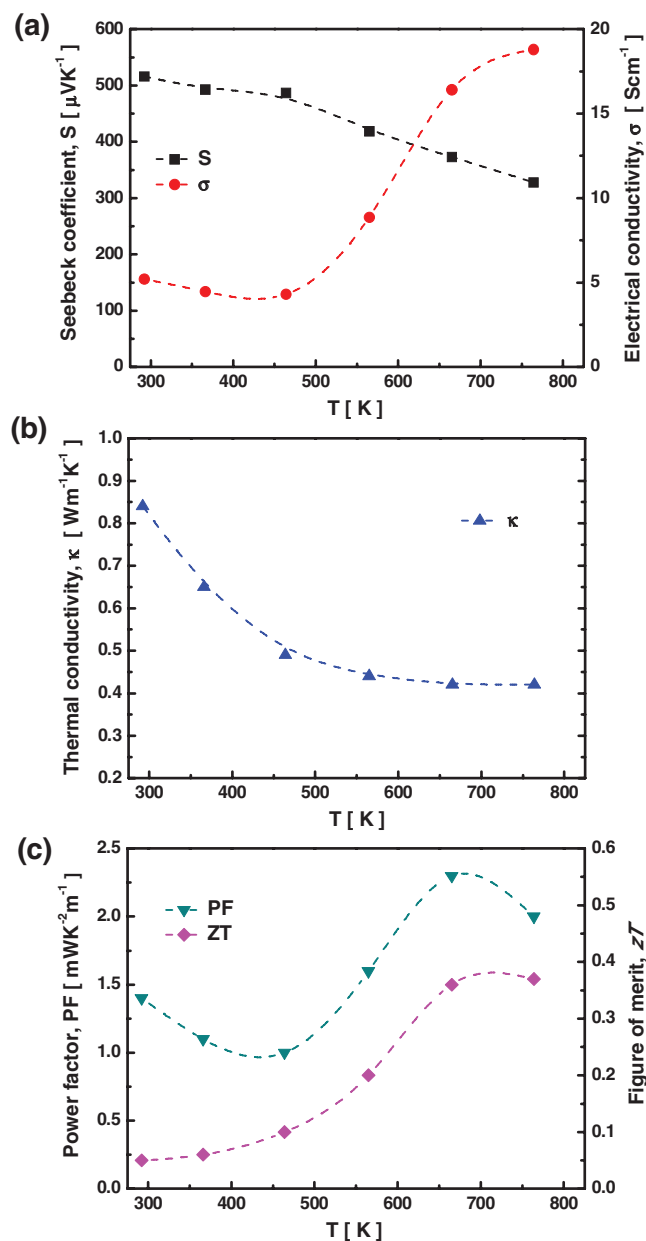
Figure 2. Temperature dependence of thermoelectric properties of the BiCuSeO after SPS treatment: a) Seebeck coefficient and electrical conductivity, b) thermal conductivity, and c) power factor and figure of merit ZT.

the BCSO pellets after spark plasma sintering (SPS). The Seebeck coefficient was highest at room temperature with a value 516 µV K^{-1}, then decreased with increasing of temperature, and reached 328 µV K^{-1} at 764 K. The electrical conductivity σ decreased with increasing temperature from room temperature to about 460 K, then increased with further increasing temperature, and reached its highest value of 18.8 S cm^{-1} at 764 K. The thermal conductivity k was found to decrease continuously with temperature, being 0.84 W m^{-1} K^{-1} at 315 K and 0.42 W m^{-1} K^{-1} at 764 K; these values are very low even for TE materials. The highest power factor ($S^2\sigma$) of 230 µW m^{-1} K^{-2} was obtained at ≈665 K. ZT values were found to increase with increasing temperature and reached 0.37 at ≈764 K. The Seebeck coefficient and electrical conductivity of the samples had lower values but similar trends with temperature as BCSO prepared using self-propagating high-temperature synthesis (SHS),[10] but higher than those of BCSO prepared using solid state reaction (SSR).[11] The thermal conductivity values were lower than both SHS and SSR prepared BCSOs.[10,11] As a result, our BCSO showed similar ZT values (0.36 at 665 K and 0.37 at 764 K) as SHS (0.33 at 675 K and 0.49 at 775 K),[10] but higher than SSR (0.09 at 725 K and 0.15 at 775 K) samples.[11]

3.2. Thin Film and Nanoparticle Catalysts on BiCuSeO

The surface microstructures of the catalysts on BCSO were investigated using scanning electron microscopy (SEM). **Figure 3** shows SEM images for the surface of: (a) BCSO, (b) Pt(15)/BCSO, (c) Pt(80)/BCSO, and (d) Pt(NP)/BCSO. Here, Pt(15), Pt(80), and Pt(NP) refer to the nominal Pt film thicknesses of 15, 80 nm, and as nanoparticles, respectively. The surface of BCSO was relatively smooth. Many Pt particles (indicated by arrow heads) could be observed on the grains of Pt(80)/BCSO and some Pt particles could be seen on the grains of Pt(15)/BCSO as well (indicated by arrow heads). Pt(NP)/BCSO had smaller grains and more voids. This was probably due to its lower sintering temperature (823 K), compared with 923 K used for the other three samples. X-ray diffraction pattern (XRD) patterns for all of the four samples are shown in Figure 3e, indicating that the BCSO in every sample was almost a single phase (PDF#45-0296) with the ZrSiCuAs structure. No second phase was observed in BCSO, but a small peak at $2\theta = 27.2$ suggested some Bi_2O_3 was present as a second phase in the other three samples. Also, the Pt(111) peak was apparent for Pt(80)/BCSO, but could not be seen in the XRD patterns for Pt(15)/BCSO and Pt(NP)/BCSO, indicating that the Pt particle sizes in the latter two samples were too small to be detected by XRD, probably less than 20 nm in diameters.

3.3. Promotion of Catalytic Activity by Thermoelectric Effect

3.3.1. The Thermoelectric and Reduced Thermoelectric (RTE) Effect Conditions

The schematic diagram of the single chamber reactor which combines TE effect with catalytic chemical reaction is shown in **Figure 4**a and Figure S1 (Supporting Information). The
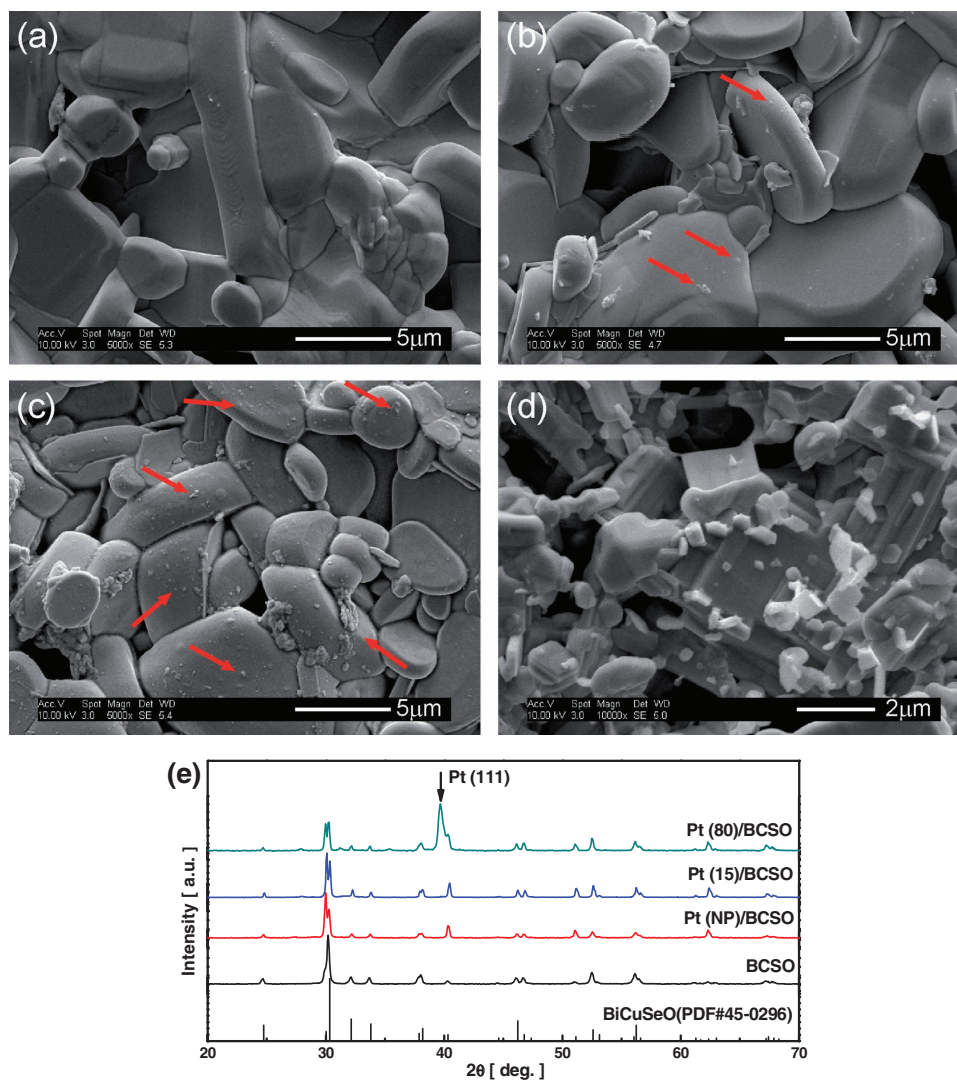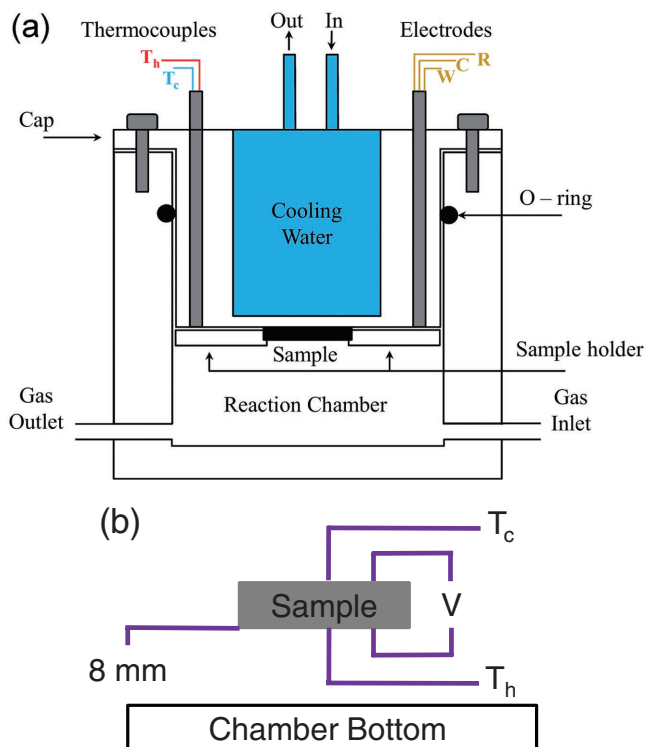
Figure 3. Microstructures for a) BCSO, b) Pt(15)/BCSO, c) Pt(80)/BCSO, d) Pt(NP)/BCSO, and e) XRD patterns after the chemical reaction measurements.

reaction chamber was placed on top of a hot-plate to create a large temperature difference (≈200–300 K when T_h > 500 K) between the bottom floor of the chamber and the hot surface T_h of the sample (Figure 4b). A large temperature gradient in the chamber can induce strong convection along the vertical direction, which can bring in the reactants and remove the products quickly from the reaction surface T_h. Figure 3a–d shows that the samples were not porous; hence, there was no pore-diffusion limitation. For these reasons, it was assumed that there was no mass transportation limitation, and the intrinsic chemical reaction was the rate limiting step for all the reactions investigated. Disc samples with a diameter of 20 mm and thickness of 2 mm were tested for catalytic activity as represented by CO_2 hydrogenation conversion X (%) at different temperatures (CO_2 conversion X is proportional to the CO_2 reaction rate r if the backward reaction of Equation (1) is ignored, this will be discussed later). Catalytic activities are then compared between the TE and RTE conditions, at the same front (hot) surface temperature. Under normal TE conditions, the backside of the

disc was in contact with water cooled stainless steel cap (with a thin mica sheet in between for electrical insulation), so its temperature was never higher than 373 K. A large temperature gradient across the disc thickness was created when the front surface reached a high temperature. Under RTE conditions, the backside of the disc was not in contact with the cooled cap, so the temperature gradient across the disc thickness was much smaller. At a particular hot-plate temperature, after reaching thermal equilibrium, the bottom surface of the disc sample was stabilized at a temperature T_h, while the top surface was at a temperature T_c. Hence, for the same sample at the same temperature T_h under TE and RTE conditions, the only differences was that the top surface temperature T_c was different, which led to a different Seebeck voltage across the sample. The Seebeck voltage V between the surfaces T_c and T_h was monitored continuously during the whole period of the experiment (Figure 4b, Figures S2 and S3 in the Supporting Information).

The CO_2 hydrogenation reactions could have taken place on the hot surface T_h (nominal surface area 100 π mm²), cold

**ADVANCED
SCIENCE NEWS**

www.advancedsciencenews.com

**ADVANCED
ENERGY
MATERIALS**

www.advenergymat.de

Figure 4. a) Schematic diagram of the single chamber reactor which can combine thermoelectric effect with catalytic chemical reaction. b) Schematic diagram of the arrangement of the sample and the measured parameters for all the catalytic reaction experiments. T_c and T_h were measured temperatures at the top and bottom surfaces of the sample, and V the corresponding Seebeck voltage. The bottom surface of the sample was about 8 mm above the bottom of the stainless steel chamber. The temperature of the chamber bottom was 200–300 K higher than the bottom of the disc sample.

surface T_c (nominal surface area 100 π mm²), and the side wall of the disc (nominal surface area 40 π mm²) sample. From Tables S1 and S2 (Supporting Information), it can be seen that when T_h was below 403 K no CO_2 conversion was obtained, and T_c was never higher than 331 K. Especially at high temperatures, T_h was much higher than T_c, and the temperature of the side wall was between T_c and T_h. For these reasons we assume that for all of the samples, the measured CO_2 conversion rate was contributed from the hot surface T_h only, and the contributions from the cold surface T_c and the side wall of the disc sample were negligible.

3.3.2. Higher Catalytic Activity at the Same Temperature under TE than RTE Conditions

The reaction products observed were only CO and CH_4, with the vast majority (>90%) being CO (**Figure 5**a). Figure 5b shows the CO_2 conversion as a function of temperature T_h under the TE and RTE conditions for Pt(80)/BCSO and BCSO with a inlet gas ratio of $CO_2/H_2 = 1:1$. It can be seen that for the same sample at the same temperature, the CO_2 conversion X under TE conditions was much greater than under RTE conditions. For example, for Pt(80)/BCSO at 573 K, the CO_2 conversion
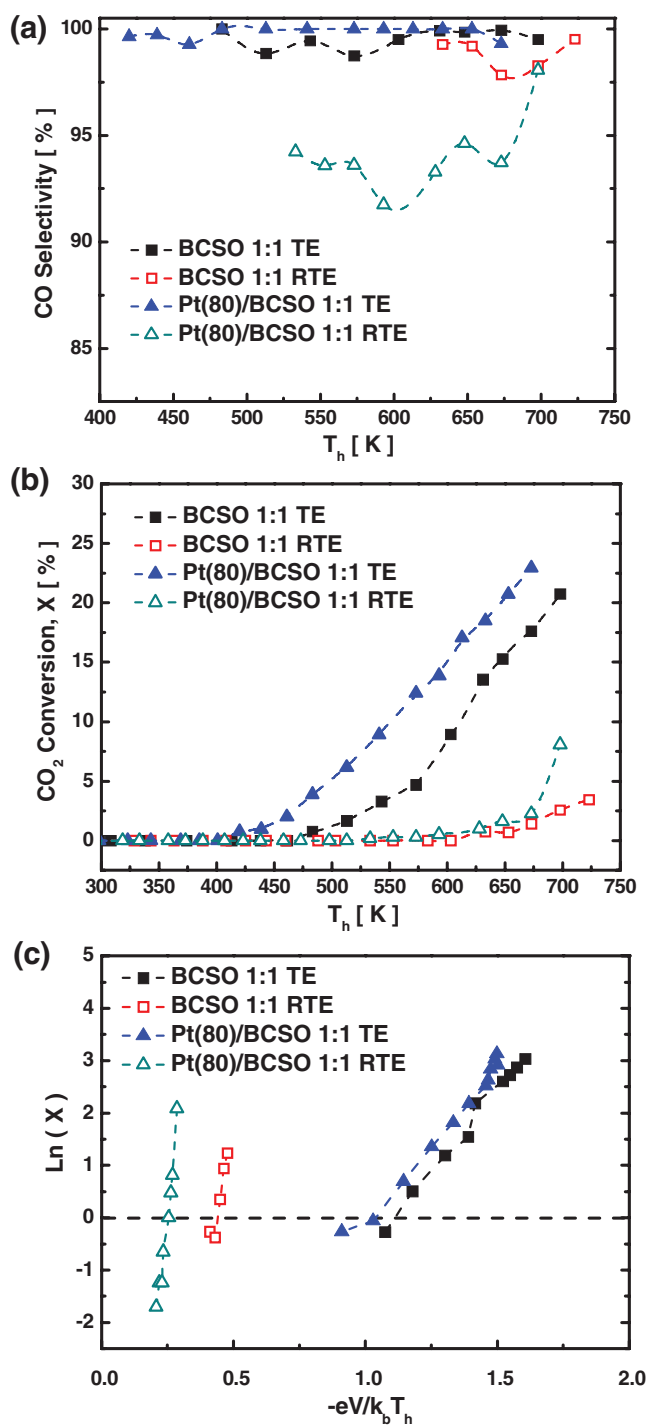
Figure 5. a) CO selectivity and b) CO_2 conversion X for Pt(80)/BCSO and bare BCSO with inlet gas ratio $CO_2/H_2 = 1:1$. For the same sample at the same temperature T_h, the conversion under large temperature gradient TE conditions was at least 10 times higher than under reduced temperature gradient RTE conditions c) a linear relationship exists between Ln(X) and $-eV/k_bT_h$.

under TE condition was 12.4%, 42 times higher than 0.3% under RTE conditions. At 673 K, the CO_2 conversion under TE condition was 10 times higher than under RTE conditions. Also, CO_2 conversion (0.8%) was first obtained at 420 K under

the TE conditions, much lower than 553 K when it was first measured under the RTE conditions (0.2%). It is plausible to assume that relative to conditions without any TE effect, the promotional effect should be even higher. It is worthy to point out that similar experiments were repeated at least once and the results were reproducible (the same samples were used for oxidized ethylene to form CO_2 and H_2O, and a repeatable and similar thermoelectric promotional effect was observed; these are the subjects for a separate publication), this ruled out the possible explanation that the conversion difference between the TE and RTE was due to the catalyst particles aggregation at the surface.

Another observation was that the BCSO TE sample, without any Pt catalyst, was also catalytically active for CO_2 hydrogenation (Figure 5b). This may not be a total surprise, as BCSO is electrically conductive, and other conductive oxides have been found to be good catalysts.[12] Moreover, Cu and CuO catalysts are widely used for CO_2 hydrogenation,[13] so the CuO containing BCSO itself could have very low catalytic activity even without thermoelectric promotion. The first measured CO_2 conversion (0.3%) was at 493 K under TE conditions and 633 K under RTE conditions (0.8%). As for Pt(80)/BCSO, at the same temperature T_h the CO_2 conversion under TE conditions was much higher than under RTE conditions. At 698 K, the CO_2 conversion was 20.8% under TE conditions compared to 3.4% under RTE conditions. Figure 5c plots Ln(X) against $-eV/k_bT_h$ for all of the cases (for the p-type BCSO, V was negative and the term $-eV$ was positive). It can be seen that a very good linear relationship existed between Ln(X) and $-eV/k_bT_h$ for each case.

3.3.3. Promotion of CO_2 Conversion by Thermoelectric Effect

To further investigate the relationships between the temperature, Seebeck voltage, and catalytic activity, the CO_2 reduction reactions were studied for different samples under different inlet gas compositions, all under TE conditions. **Figure 6**a displays the measured thermoelectric voltage as a function of the temperature difference ΔT across the sample thickness for four samples, namely Pt(80)/BCSO, Pt(15)/BCSO, Pt(NP)/BCSO, and bare BCSO, at the inlet gas ratios of $CO_2/H_2 = 1:1$ and 1:4. All of the four samples were weighted as 5.8 g. All of the samples had zero voltages when their bottom and top surfaces were at the same (room) temperature. The measured voltage for each sample increased linearly with temperature difference. The linear gradient for Pt(80)/BCSO was 319 μV K^{-1} for ΔT < 200 K, and then decreased with increasing ΔT. The gradients for BCSO and Pt(15)/BCSO were similar and did not change with the change of the inlet gas compositions. These are typical values for Seebeck coefficient of BCSO.[2] Note that the Seebeck coefficient of 319 μV K^{-1} here is lower than the values reported in Figure 2a for SPS processed material. The main reason for this was that the BCSO used for the above catalysis experiments was not densified by SPS but using conventional sintering, so an inferior crystallinity and density of this sample was expected, which led to a smaller Seebeck coefficient. Another reason was that the Seebeck coefficient obtained through the linear gradient here was the average value over a large temperature range, while those in Figure 2a were obtained by changing the temperature over a smaller range (≈50 K over a 13 mm long sample), and generally speaking,
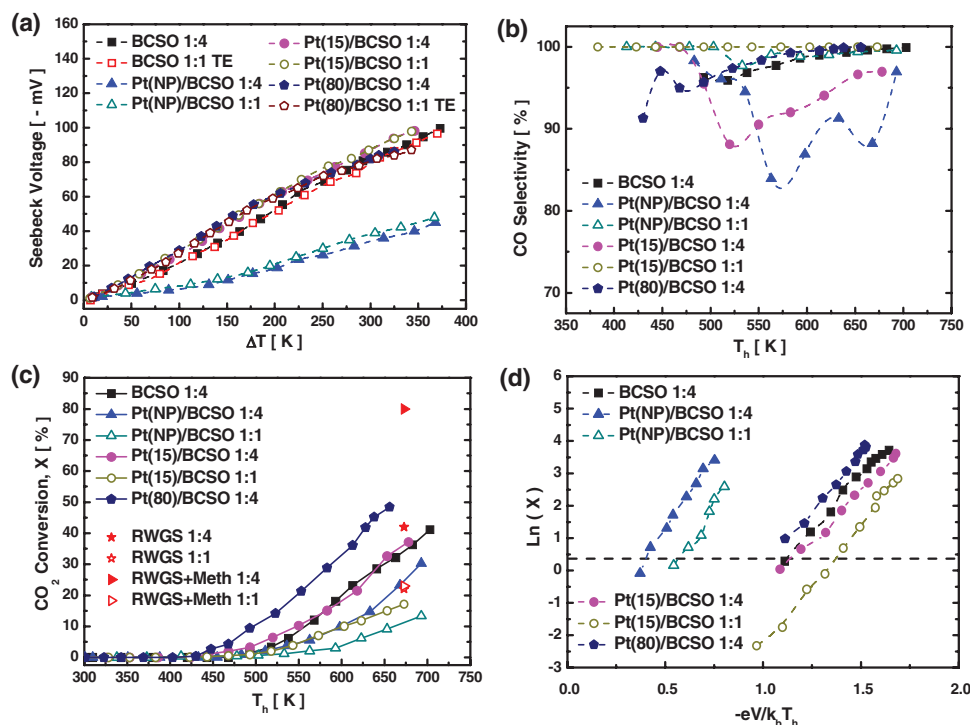
Figure 6. Thermoelectric promotion of catalytic CO_2 hydrogenation on Pt and TE materials BCSO. a) Measured voltages as functions of temperature difference across the sample thickness. b) CO selectivity as functions of temperature. c) CO_2 conversion rate X increased with temperature T_h. d) a linear relationship exists between Ln(X) and $-eV/k_bT_h$.

**ADVANCED
SCIENCE NEWS**

www.advancedsciencenews.com

**ADVANCED
ENERGY
MATERIALS**

www.advenergymat.de

the Seebeck coefficient is temperature dependent. The gradient for the Pt(NP)/BCSO was much lower, at about 136 µV K^{-1}, again, it also kept the same value when the inlet gases ratio was changed from 1:1 to 1:4. This much lower Seebeck coefficient was due to the fact that this sample was sintered at a much lower temperature (823 K as compared to 923 K for other BCSO), and there were still some second phases such as Bi_2O_3 and void in the sample (Figure 3d). These results demonstrate that the measured voltage was determined by the intrinsic thermoelectric properties of the sample and the temperature difference only, and was not affected by the gas compositions.

Again, the reaction products were found to be CO and CH_4, with the majority (>80%) being CO. Higher H_2 concentration in the inlet gases led to lower CO selectivity. The temperature dependences of CO selectivity for six cases are shown in Figure 6b, while the other two, BCSO 1:1 TE and Pt(80)/BCSO 1:1 TE, are shown in Figure 5a. Generally speaking, at $T > 600$ K, the CO selectivity increased with temperature and voltage. Figure 6c shows the CO_2 conversion as a function of the hot-surface temperature T_h for different samples at the inlet gas ratios of $CO_2/H_2 = 1:1$ or 1:4. All of the samples showed a similar trend, i.e., the conversion increased with temperature. It can be seen that for the same sample, higher H_2 concentration leads to higher CO_2 conversion. Pt(80)/BCSO reached 48.4% conversion at 656 K, the highest for all of the samples, indicating that the Pt surface had the highest catalytic activity. Remarkably, even without any Pt catalyst, the TE material BCSO ($CO_2/H_2 = 1:4$) itself reached a conversion of 41.2% at 703 K.

Excellent linear relationships were observed between Ln(X) and $-eV/k_bT_h$ for all ten cases (four for Figure 5c and six for Figure 6d). The best-fit trend line gradients γ were obtained as: 6.6 for BCSO @ 1:4 and 6.22 for BCSO @1:1 TE; 6.06 for Pt(15)/BCSO @ 1:4 and 7.46 for Pt(15)/BCSO @ 1:1; 7.2 for Pt(80)/BCSO @1:1 and 7.15 for Pt(80)/BCSO @ 1:4; 9.09 for Pt(NP)/BCSO @1:4 and 9.73 for Pt(NP)/BCSO @1:1; 46 for Pt(80)/BCSO @ 1:1 RTE and 25.4 for BCSO @ 1:1 RTE. Generally speaking, as can be seen from Figures 5c and 6d, γ had similar values for all the TE conditions and much higher values for the RTE conditions.

Combining the results as shown in Figures 5c and 6d, we can summarize the observed relationship in Equation (7)

$$Ln(X/X_0) = -\gamma eV/k_bT_h \qquad (7)$$

Here, X_0 is the conversion rate when V equals zero, i.e., when $T_c = T_h$. For the p-type TE material BSCO, V at T_h surface is negative, so $-\gamma eV$ is positive and the conversion rate at the hot side T_h could be much higher with a TE voltage than without, we call this thermoelectric promotion of catalysis (TEPOC), or thermoelectrocatalysis as the TE material itself can be catalytic active. Take an experimental data point for Pt(80)/BCSO @ 1:4, $T_h = 656$ K, $V = -86$ mV, and $\gamma = 7.15$, so Ln(X/X_0) = $-\gamma eV/k_bT_h$ = 10.88, and $X/X_0 = 53103$. This means that at 656 K, the conversion with a Seebeck voltage of -86 mV was more than 53 thousand times higher than without a Seebeck voltage.

Equation (4) can lead to Equation (7), and vice versa, if the conversion X is proportional to the reaction rate r. This requires

the conversion X to be much lower than the thermal equilibrium conversion (TEC) of the reactions in Equation (1) and Equation (2), so that the backward reactions were negligible. The TECs at 673 K for CO_2 conversion in RWGS reaction without methanation (to CO only) are about 22% and 42% for an inlet gas ratio $CO_2/H_2 = 1:1$ and 1:4 respectively; with methanation, the corresponding values are about 23% and 80%, respectively.[14,15] Under RTE conditions, the conversion rate was very low; hence, the CO_2 conversion on both Pt(80)/BCSO and BCSO was far away from the TEC, so it is safe to assume that the backward water-gas shift reaction can be ignored and the CO_2 conversion X was linearly proportional to the reaction rate r. So for the two cases under RTE conditions, the experimental results confirmed the prediction of Equation (4).

The rate of chemical reactions usually follows the Arrhenius law, so $r_0 = k_0 \exp(-E_a/k_bT_h)$, here k_0 is a constant, E_a the activation energy of the reaction. Equations (4) and (7) apparently suggest that the activation energy is reduced by $-\gamma eV$, i.e., $E'_a = E_a + \gamma eV$, E'_a is the new activation energy when there is a TE voltage V (a negative value for our case, as the reaction take place at the hot side of a p-type TE material).

Figures 5b and 6c show that at high temperatures around 673 K, when there was a high Seebeck voltage, the CO_2 conversion rate reached TEC (22.9% for Pt(80)/BCSO @ 1:1 TE at 673 K), or just slightly below TEC (17.6% for BCSO @ 1:1 TE at 673 K, 37.2% for Pt(15)/BCSO @ 1:4 at 678 K, 36.3% for BCSO 1:4 at 683 K), even above the TEC (48.4% for Pt(80)/BCSO 1:4 at 656 K) without methanation. For the purpose of comparison, the TEC values for CO_2 conversion in RWGS reactions with and without methanation at CO_2/H_2 ratios 1/1 and 1/4 at 673 K are also presented in Figure 6c. To the best of our knowledge, 48.4% is the highest reported CO_2 conversion to CO (with 100% CO selectivity) at atmosphere pressure below 673 K with an inlet gas ratio CO_2/H_2 no larger than 4.[13,15,16] How can the CO_2 conversion to CO exceeds the TEC at 673 K? It can be seen from Figure 6b that at temperatures $T_h > 678$ K, the CO selectivity was >95% for all the samples. Notably for Pt(80)/BCSO @ 1:4, the CO selectivity was 100% at 656 K. The CO selectivities observed at these temperatures were also much higher than the predicted values under the consideration of thermal equilibrium.[13,15,16] These results indicate that the Seebeck voltage promoted the conversion to CO and forward reaction in Equation (1), hence changed the TEC. This agrees with the observation that an electric field (via the NEMCA mechanism) shifted the chemical equilibrium, increased the RWGS reaction, and decreased the (backward) water-gas shift reaction.[15] With the assistance of an electric voltage of 1.6 kV, CO_2 conversion to CO on a Pt/La-ZrO_2 catalyst reached 40.6% with an inlet gas ratio $CO_2/H_2 = 1:1$ at 648 K, much higher than the TEC of about 20% without electric field at the same temperature.[15] This shifted the chemical equilibrium and TEC by an electrochemical energy of $-eV$ and may also be the reason why we observed the linear relationships in Figures 5c and 6d. Strictly speaking, if the conversion rate is close to the TEC and the backward water-gas-shift reaction cannot be ignored, and the conversion X is not determined by the reaction rate, and Equation (4) cannot lead to Equation (7). Nevertheless, a very good linear relationship between Ln(X) and $-eV/k_bT_h$ was observed for all the cases investigated. The most plausible

explanation is that the Seebeck voltage V (or electrochemical energy $-eV$) shifted the reactions in Equation (1) toward the forward reaction, i.e., the RWGS against the backward water-gas shift reaction. Hence, the achieved conversion rate was still far away from the new chemical equilibrium and Equation (7) can still be explained by Equation (4).

3.4. Discussion

Referring to Figure 6a,c,d, all the samples, either bare BSCO or BCSO with a continuous Pt thin film Pt(80)/BCSO, or BCSO with discontinuous Pt nanoparticles Pt(15)/BCSO and Pt(NP)/BCSO, showed similar CO_2 conversion dependence with the temperature T_h and Seebeck voltage V (Figures S4 and S5, Supporting Information). The four samples with similar Seebeck voltage at a particular temperature, i.e., BCSO @4, Pt(15) BCSO @1:1, Pt(15)/BCSO @1:4, and Pt(80)/BCSO @1:4, also had similar $Ln(X) \sim -eV/k_b T_h$ relationships. The sample Pt(NP)/BCSO @ 1:1 and 1:4 had the lowest Seebeck voltage and also had a similar $Ln(X) \sim -eV/k_b T_h$ relationship. This suggests that the Seebeck voltage, not specific surface property, was the most important factor in determining the catalytic activity. This also agrees with the observation that the CO_2 conversion stronger dependence on the effect of the electric field than the nature of the catalyst.[15] These results also agree with the observations in NEMCA of CO_2 hydrogenation in that a negative (reduced) potential increased the selectivity and reaction rate to CO, and a positive (increased) potential increased the selectivity and reaction rate to CH_4.[13,17]

From the above discussion, all the above observed results can be explained by Equation (4), i.e., the change of work function lead to the promotion of catalytic activity. This mechanism based on the change of work function through the in situ and controlled TE effect suggests that TEPOC is an effective mechanism for any metallic catalysts, regardless of their properties such as particle size or total amount of the metal. This is because whatever the particle size or chemisorption property, the Fermi level of the metallic particle will be the same as that of the surface TE materials supporting them. The total amount of the metal particles, indeed any second phase materials, will affect the TE properties such as Seebeck coefficient and electrical conductivity, as the whole system can be regarded as a TE composite. This is because all of the samples, with or without metal Pt, are just thermoelectric materials with a different Seebeck coefficient. Of course, the metal particle surface and TE surface may have different adsorption properties, which may lead to different catalytic properties.

Since the TE effect can be realized independently of chemical reactions, its modification to the catalytic activity can be in situ under operational conditions, and controlled through the control of the backside temperature, e.g., changing the water cooling to liquid nitrogen cooling. For n-type TE materials, the Fermi level at the cold side is higher than at the hot side, but the relationship $\varepsilon_{F,h} - \varepsilon_{F,c} = -eV$ is still valid, so is $\Delta\phi = eV$, but V is now positive.

The significant promotional effect of the TE effect when there is a large Seebeck voltage can be understood from the energy point of view. $-eV/k_b T_h$ can be regarded as the ratio between the extra electrochemical energy induced by TE effect and the thermal energy of an electron at the reaction surface. At 300 K, the thermal energy $k_b T$ is 25.9 meV. So, 104 mV of Seebeck voltage gives 104 meV extra electrochemical energy to an electron at the Fermi level, which is equivalent to the thermal energy of an electron at 1200 K, but a 104 mV Seebeck voltage can be generated by a temperature difference of 347 K by a TE material (such as BCSO) with an average Seebeck coefficient of 300 μV K^{-1}. So, TE effect is a very efficient way to enhance the electrochemical energy of an electron at the reaction surface.

Considering $\Delta\phi = eV$ in TEPOC, note that Equation (4) is similar to the rate equation for NEMCA,[3,8,9] which is $Ln(r/r_o) = \alpha(\Delta\phi - \Delta\phi^*)/k_b T$, where r_o is the open-circuit reaction rate, α and $\Delta\phi^*$ are empirically determined constants, $\Delta\phi$ is the change of work function due to the applied external voltage. Under certain conditions, $\Delta\phi$ is linearly proportional to the non-Ohm drop of external potential,[3,8] so the rate Equation (4) for TEPOC looks exactly the same as the rate equation for NEMCA. However, there are a few important differences between NEMCA and TEPOC. (i) No electrolyte nor external voltage are needed in the TEPOC system, while for NEMCA, an electrical insulating electrolyte layer is crucial otherwise a non-Ohm drop of potential (or ionic current) cannot be established. In fact, the unusually low thermal conductivity of BCSO has been attributed to its negligible ionic conductivity, so the back spill-over of ionic species in BCSO would have been negligible.[18] Also, we did not observe any change of reaction rate when an external voltage (positive or negative) was applied to the Pt(80)/BCSO or other samples. (ii) Unlike in NEMCA, the catalyst in TEPOC (e.g., Pt) does not need to be continuous, as TE materials are electrically conductive. Highly, separately dispersed catalysts, including nanoparticle catalysts, can be promoted by TEPOC. (iii) The constant α in NEMCA is smaller than unity, but the values for the constant γ in TEPOC have been found to be larger than 1. The fact that $\gamma > 1$ in the Equations (4)–(7) for TEPOC indicates that there is an amplification effect when the extra electrochemical energy eV is present during catalytic chemical reactions. The mechanism for this is not clear yet, but we speculate that this is related to the increase of the number of electrons available for catalytic reaction with the increasing temperature, as no change of electron density with temperature should mean $\gamma = 1$. (iv) The TE material itself can be used as a catalyst when there is a large Seebeck voltage. (v) Furthermore, more importantly, the mechanism for the change of work function at the catalyst surface in TEPOC is different from that in NEMCA. In NEMCA, the external voltage induces the diffusion of ionic species, which form a double layer on the catalyst surface, and produce a change of the work function.[3,8] Hence, the change of work function $\Delta\phi$ is an indirect consequence of the external voltage V, and the linear relationship between $\Delta\phi$ and V is true only under certain conditions and may be sample dependent.[19] In TEPOC, the relationship between $\Delta\phi$ and Seebeck voltage V is directly linked by the change of Fermi level, not through the formation of a double layer.

4. Conclusions

The thermoelectric oxide BiCuSeO has been produced using a facile solid state reaction method using B_2O_3 as a flux agent in

air. An innovative use of the thermoelectric material as a catalyst support and promoter has been proposed and investigated through the CO_2 hydrogenation to produce CO and CH_4. A very high CO_2 conversion of 48.4% to CO with 100% CO selectivity under atmosphere at temperatures below 673 K with the inlet gas ratio $CO_2/H_2 = 1:4$ was obtained.

It is proposed that the thermoelectric effect can change the Fermi level and therefore the work function of the electrons in the catalyst particles supported on a thermoelectric material. This change of work function leads to exponential increase of catalytic activity. It was indeed observed in experiments that the catalytic activity of metallic particles supported on the thermoelectric materials, as represented by the CO_2 conversion, was significantly promoted by a Seebeck voltage generated through a temperature difference across the thickness of the thermoelectric support. This thermoelectric promotion of catalysis also enabled the BiCuSeO itself to possess high catalytic activity. It was further confirmed by experimental results that there exists a linear relationship between the logarithm of the catalytic activity, and $-eV/k_bT$, which can be regarded as the ratio of extra electrochemical energy $(-eV)$ induced by thermoelectric effect and thermal energy (k_bT) of an electron. This extra electrochemical energy can also change the chemical equilibrium and selectivity of the reaction.

The general nature of the mechanism suggests that thermoelectric promotion of catalysis could be a universal phenomenon.

5. Experimental Section

Thermoelectric Material Preparation: The TE material BCSO was synthesized by solid-state reaction using boron oxide (B_2O_3, Alfa Aesar, 99%) as a flux agent in air. During the flux synthesis, the melted B_2O_3 served as a liquid-seal on the top of the crucible. The obtained product of each sample was then ground to a fine powder. The latter was densified at 150 MPa using a hydraulic press system to form a dense pellet of 20 mm in diameter and 2 mm in thickness. Then, the green pellet was sintered at 923 K for 10 h under an argon atmosphere. Further sintering by SPS was carried out before thermoelectric property measurements, using a HP D 25/1(FCT Systeme GmbH, Frankenblick, Germany).

Preparation of Catalysts: The film catalysts were deposited on BCSO by magnetron sputtering method (Nordiko). The Pt films were prepared using pure Pt (99.99%) as the sputtering target. The thicknesses of the Pt films were ≈80 nm for three min and ≈15 nm for 20 s of sputtering time, respectively named Pt(80)/BCSO and Pt(15)/BCSO. Another platinum nanoparticle sample (Pt(NP)/BCSO) was synthesized using an impregnation method. For this sample, the green pellet was calcined at 823 K for 2 h under argon atmosphere and then reduced under 5% H_2 in Ar at 773 K for 4 h.

The microstructural investigations were carried out using XRD (Siemens 5005) at 40 kV with a Cu Kα source and a scanning electron microscope (Philips, FEI XL30 SFEG).

Thermoelectric Property Measurements: The thermal diffusivity (D) was measured by using laser flash method (LFA-457, Netzsch, Germany) under a continuous argon flow. The total thermal conductivity (κ_{total}) was calculated by the formula $\kappa = DC_p\rho$, where ρ was the mass density measured by the Archimedes method, while the specific heat (C_p) was determined using a differential scanning calorimeter instrument. The electrical conductivity and Seebeck coefficient were simultaneously measured (LSR-3/1100, Linseis) in a He atmosphere.

The Reaction Chamber: Chemical reactions were performed in a single chamber reactor. A schematic diagram of the reactor can be seen in Figure 1. The cover plate was cooled with continuous running water. Gold wires (Agar Scientific, Ø 0.2 mm) were used as electrical contacts, and temperatures were measured with K-type thermocouples (Ø 0.25 mm, TC Direct) placed directly on the sample surfaces. The reaction chamber was placed directly onto a high temperature hot plate (HP99YX, Wenesco, Inc.) with a temperature controller. The Seebeck voltage was measured continuously (Figures S1 and S2, Supporting Information) between the bottom surface and the top electrode (Au) using a potentiostat–galvanostat (VersaStat 3F, Princeton Applied Research).

Catalytic Activity Measurement: The catalytic activity measurements of different catalysts were carried out at atmospheric pressure in a continuous flow apparatus equipped with the stainless steel reactor (Figure 1b). The reaction reactants and products were continuously monitored using online gas chromatography (GC8340, CE instruments) and online IR analyzer (G150 CO_2, Gem Scientific) to quantify the concentration of H_2, CO, CH_4, and CO_2. To monitor the temperature, a K-type thermocouple was attached (and fixed using a high temperature tape) onto the catalyst surface for the T_h measurement. Another K-type thermocouple was placed in proximity of the top surface for the T_c measurement. Carbon mass balance for all of the experiments was found to be within 6%.

The catalyst activities were investigated with the composition of carbon dioxide and hydrogen at a ratios of CO_2:H_2 = 1:1, and CO_2:H_2 = 1:4. All samples were tested at an overall flow rate of 100 mL min^{-1}.

The conversion of CO_2 and the selectivity of CO and CH_4 were evaluated from the outlet carbon percentage values obtained by the gas analysis. H_2O vapor was condensed before entering the GC to prevent deterioration of the GC column. CO_2 conversion X_{CO_2}, and the selectivity of CO and CH_4 were calculated as

$$CO_2 \text{ Conversion} \% = \frac{\gamma_{CO} + \gamma_{CH_4}}{\gamma_{CO} + \gamma_{CH_4} + \gamma_{CO_2}} \times 100 \tag{8}$$

$$CO \text{ Selectivity} \% = \frac{\gamma_{CO}}{\gamma_{CO} + \gamma_{CH_4}} \times 100 \tag{9}$$

$$CH_4 \text{ Selectivity} \% = \frac{\gamma_{CH_4}}{\gamma_{CO} + \gamma_{CH_4}} \times 100 \tag{10}$$

where γ_{CO_2}, γ_{CO}, and γ_{CH_4} were the mol fractions of CO_2, CO, and CH_4 in the outlet, respectively.

$r_{CO_2} = \frac{X_{CO_2} \times f_v}{22400 \times 60}$, where $f_v = 100$ mL min^{-1} is the volumetric flow rate at the outlet of the reactor and r_{CO_2} is the CO_2 reaction rate.

Supporting Information

Supporting Information is available from the Wiley Online Library or from the author.

Acknowledgements

their contribution to this work. The authors also thank Drs. C. Shaw, X. Liu, A. Stallard, and T. Pryor for technical help.

Conflict of Interest

The authors declare no conflict of interest.

Keywords

[1] a) T. C. Harman, P. Taylor, M. Walsh, B. Laforge, *Science* **2002**, *297*, 2229; b) K. Hsu, S. Loo, F. Guo, W. Chen, J. Dyck, C. Uher, T. Hogan, E. Polychroniadis, M. Kanatzidis, *Science* **2004**, *303*, 818.

[2] a) H. Ohta, K. Sugiura, K. Koumoto, *Inorg. Chem.* **2008**, *47*, 8429; b) J. He, Y. Liu, R. Funahashi, *J. Mater. Res.* **2011**, *26*, 1762; c) C. Barreteau, L. Pan, E. Amzallag, L. Zhao, D. Berardan, N. Dragoe, *Semicond. Sci. Technol.* **2014**, *29*, 064001; d) C. Barreteau, D. Berardan, N. Dragoe, *J. Solid State Chem.* **2015**, *222*, 53; e) L. Zhao, J. He, D. Berardan, Y. Lin, J. Li, C. Nan, N. Dragoe, *Energy Environ. Sci.* **2014**, *7*, 2900; f) F. Li, T. Wei, F. Kang, J. Li, *J. Alloys Compd.* **2014**, *614*, 394; g) W. Wunderlich, T. Mori, O. Sologub, *Mater. Renew. Sustain Energy* **2014**, *3*, 21.

[3] C. G. Vayenas, S. Bebelis, C. Pliangos, S. Brosda, D. Tsiplakides, *Electrochemical Activation of Catalysis: Promotion, Electrochemical Promotion, and Metal-Support Interactions*, Kluwer Academic, New York **2001**.

[4] a) D. Poulidi, C. Anderson, I. Metcalfe, *Solid State Ionics* **2008**, *179*, 1347; b) M. Konsolakis, N. Macleod, J. Isaac, I. Yentekakis, R. Lambert, *J. Catal.* **2000**, *193*, 330; c) A. de Lucas-Consuegra, J. González-Cobos , Y. Gacia-Rodriguez, J. L. Endrino, J. L. Valverde, *Electrochem. Commun.* **2012**, *19*, 55; d) A. de Lucas-Consuegra, J. González-Cobos, Y. García-Rodríguez, A. Mosquera, J. L. Endrino, J. L. Valverde, *J. Catal.* **2012**, *293*, 149; e) A. Kambolis, L. Lizarraga, M. Tsampas, L. Burel, M. Rieu, J. Viricelle, P. Vernoux, *Electrochem. Commun.* **2012**, *19*, 5; f) I. R. Harkness, C. Hardacre, R. M. Lambert,

I. V. Yentekakis, C. G. Vayenas, *J. Catal.* **1996**, *160*, 19; g) Z. Wang, H. Huang, H. Liu, X. Zhou, *Int. J. Hydrogen Energy* **2012**, *37*, 17928.

[5] D. Tsiplakides, S. Balomenou, *Chem. Ind. Chem. Eng. Q.* **2008**, *14*, 97.

[6] K. A. Bishop, A. M. Betzelberger, S. P. Long, E. A. Ainsworth, *Plant, Cell Environ.* **2015**, *38*, 1765.

[7] a) G. A. Olah, G. Prakash, A. Goeppert, *J. Am. Chem. Soc.* **2011**, *133*, 12881; b) W. Wang, S. Wang, X. Ma, J. Gong, *Chem. Soc. Rev.* **2011**, *40*, 3703; c) J. Ma, N. Sun, X. Zhang, N. Zhao, F. Xiao, W. Wei, Y. Sun, *Catal. Today* **2009**, *148*, 221; d) B. Hu, C. Guild, S. Suib, *J. CO2 Util.* **2013**, *1*, 18; e) H. Jhong, S. Ma, P. Kenis, *Curr. Opin. Chem. Eng.* **2013**, *2*, 191; f) G. A. Olah, *Catal. Lett.* **2004**, *1*, 93; g) N. Hollingsworth, R. Taylor, M. T. Galante, J. Jacquemin, C. Longo, K. B. Holt, N. Leeuw, C. Hardacre, *Faraday Discuss.* **2015**, *183*, 389.

[8] C. G. Vayenas, S. Brosda, C. Pliangos, *J. Catal.* **2003**, *216*, 487.

[9] C. G. Vayenas, S. Bebelis, S. Ladas, *Nature* **1990**, *343*, 625.

[10] G.-K. Ren, J.-L. Lan, S. Butt, K. J. Ventura, Y.-H. Lin, C.-W. Nan, *RSC Adv.* **2015**, *5*, 69878.

[11] J. Li, J. Sui, Y. Pei, X. Meng, D. Berardan, N. Dragoe, W. Cai, L.-D. Zhao, *J. Mater. Chem. A* **2014**, *2*, 4903.

[12] J. Nicole, D. Tsiplakides, S. Wodiunig, Ch. Comninellis, *J. Electrochem. Soc.* **1997**, *144*, L312.

[13] E. I. Papioannou, S. Souentie, A. Hammad, C. G. Vayenas, *Catal. Today* **2009**, *146*, 336.

[14] a) A. G. Kharaji, A. Shariati, M. Ostadi, *J. Nanosci. Nanotechnol.* **2014**, *14*, 1; b) R. B. Unde, *Kinetics and Reaction Engineering Aspects of Syngas Production by the Heterogeneously Catalysed Reverse Water Gas Shift Reaction, Ph.D. Thesis*, University of Bayreuth, **2012**.

[15] K. Oshima, T. Shinagawa, Y. Nogami, R. Manabe, S. Ogo, Y. Sekine, *Catal. Today* **2014**, *232*, 27.

[16] a) Y. A. Daza, J. N. Kuhn, *RSC Adv.* **2016**, *6*, 49675; b) R. V. Goncalves, L. R. Vono, R. Wojcieszak, C. S. B. Dias, H. Wender, E. Teixeira-Neto, L. M. Rossi, *Appl. Catal., B* **2017**, *209*, 240; c) V. Jiménez, C. Jiménez-Borja, P. Sánchez, A. Romero, E. I. Papaioannou, D. Theleritis, S. Souentie, S. Brosdac, J. Valverde, *Appl. Catal., B* **2011**, *107*, 210.

[17] a) M. Makri, A. Katsaounis, C. G. Vayenas, *Electrochim. Acta* **2015**, *179*, 556; b) I. Kalaitzidou, A. Katsaounis, T. Norby, C. G. Vayenas, *J. Catal.* **2015**, *331*, 98.

[18] a) P. Vaqueiro, R. Al Orabi, S. Luu, S. Guelou, A. Powell, R. Smith, J. Song, D. Wee, M. Fornari, *Phys. Chem. Chem. Phys.* **2015**, *40*, 31735; b) L. Zhao, J. Li, in *BiCuSeO: A Promising Thermoelectric Material, in Materials Aspect of Thermoelectricity* (Ed. C. Uher), CRC Press, Boca Raton, FL **2016**.

[19] I. Metcalfe, *J. Catal.* **2001**, *199*, 259.